Polar Magnet

Magnetic-Structure-Stabilized Polarization in an Above-Room-Temperature Ferrimagnet[**]

Man-Rong Li, Maria Retuerto, David Walker, Tapati Sarkar, Peter W. Stephens, Swarnakamal Mukherjee, Tanusri Saha Dasgupta, Jason P. Hodges, Mark Croft, Christoph P. Grams, Joachim Hemberger, Javier Sánchez-Benítez, Ashfia Huq, Felix O. Saouma, Joon I. Jang, and Martha Greenblatt*

Abstract: Above-room-temperature polar magnets are of interest due to their practical applications in spintronics. Here we present a strategy to design high-temperature polar magnetic oxides in the corundum-derived $A_2BB'O_6$ family, exemplified by the non-centrosymmetric (R3) Ni_3TeO_6-type $Mn^{2+}_2Fe^{3+}Mo^{5+}O_6$, which shows strong ferrimagnetic ordering with $T_C = 337 K$ and demonstrates structural polarization without any ions with $(n-1)d^{10}ns^0$, d^0, or stereoactive lone-pair electrons. Density functional theory calculations confirm the experimental results and suggest that the energy of the magnetically ordered structure, based on the Ni_3TeO_6 prototype, is significantly lower than that of any related structure, and accounts for the spontaneous polarization ($68\,\mu C\,cm^{-2}$) and non-centrosymmetry confirmed directly by second harmonic generation. These results motivate new directions in the search for practical magnetoelectric/multiferroic materials.

The design of polar and magnetic materials with magneto-electric/multiferroic behavior is a key issue to develop spintronic devices for nonvolatile memories, faster data processing speeds with less power usage, larger storage densities, and additional functionalities.[1,2] There are now several demonstrated strategies to achieve electric polarization of magnetic compounds, including the lone-pair-electron-active cation,[3] charge ordering,[4] and magnetic-structure (spin spiral)[5]-driven multiferroics, the strain-induced thin film technique,[6] and polarization from geometric structure distortion,[7] including second-order Jahn–Teller (SOJT) distortion[8] and the recently predicted hybrid improper ferro-electricity in corner-sharing BO_6 network with "layered" A/A′ cations in perovskite,[9a,b] Ruddlesden–Popper,[9b,c] and Dion–Jacobson[9d] phases. So far, most of the materials-by-design work has focused on ABO_3 perovskites and related phases with either $(n-1)d^{10}ns^{0}$,[10] d^0,[7] or stereoactive lone-pair electron configuration cations,[3] to favor hybridization

[*] Dr. M. R. Li, M. Retuerto, T. Sarkar, M. Greenblatt
Department of Chemistry and Chemical Biology, Rutgers
The State University of New Jersey
610 Taylor Road, Piscataway, NJ 08854 (USA)
E-mail: martha@rutchem.rutgers.edu

Dr. D. Walker
Lamont-Doherty Earth Observatory, Columbia University
61 Route 9W, Palisades, NY 10964 (USA)

Dr. P. W. Stephens
Department of Physics & Astronomy, State University of New York
Stony Brook, NY 11794 (USA)

Dr. S. Mukherjee, T. S. Dasgupta
Department of Condensed Matter Physics and Materials Sciences
S. N. Bose National Centre for Basic Sciences
JD Block, Sector III, Salt Late, Kolkata 700098 (India)

Dr. J. P. Hodges, A. Huq
Spallation Neutron Source, Oak Ridge National Laboratory
Oak Ridge, TN 37831 (USA)

Dr. M. Croft
Department of Physics and Astronomy, Rutgers
The State University of New Jersey
136 Frelinghuysen Road, Piscataway, NJ 08854 (USA)

Dr. C. P. Grams, J. Hemberger
II. Physikalisches Institut, Universität zu Köln
50937 Köln (Germany)

Dr. J. Sánchez-Benítez
Departamento de Química Física I, Facultad de Ciencias Químicas
Universidad Complutense de Madrid
28040 Madrid (Spain)

Dr. F. O. Saouma, J. I. Jang
Department of Physics, Applied Physics and Astronomy
Binghamton University
P.O. Box 6000, Binghamton, NY 13902 (USA)

between the metal open-shell d and oxygen 2p states,[11a] or provide ferroelectrically active electron pairs.[11b] In most observed cases the multiferroic order is well below room temperature (RT); only a few candidates, such as the hexaferrites and related phases,[12a] $BiFeO_3$,[3] Cr_2O_3,[12b] ε-Fe_2O_3, and its doped analogues,[12c] show promising magneto-electric phenomena above RT. Therefore, new practical magnetoelectric materials are needed.

Recently, the corundum-derived $A_2BB'O_6$ oxides with unusually small A-site cations have drawn much attention,[13a,b] particularly Ni_3TeO_6, which was reported to show nonhysteretic colossal magnetoelectricity.[13b] The crystal structure of $A_2BB'O_6$ (Figure S1 in the Supporting Information, SI) makes it possible to incorporate strong magnetic transition metal ions on both the A- and B-sites for magnetic and potential magnetoelectric behavior. A good example is our discovery of $Mn^{2+}_2Fe^{3+}M^{5+}O_6$ (M = Nb^{5+} and Ta^{5+}; d^0 ions), with $LiNbO_3$ (LN)-type polar structures, antiferromagnetic ($T_N \approx 90$ K) ordering, spin localization, and structural distortions that predict many more interesting and useful polar magnetic phases.[13a] Therefore, it appeared promising to design above-RT polar ferri- or ferromagnets by composition modulation. In this work, we introduced Mo^{5+} into the B'-site of Mn_2FeMoO_6, and studied its crystal structure, oxidation states, optical second harmonic generation (SHG) activity, and the magnetic and electrical properties. Theoretical calculations were also performed for further insight into structure–property relationships. We have found a new magnetic and polar phase without lone-pair-electron or d^0 configuration cations, or incommensurate or helicoidal magnetic structures. Mn_2FeMoO_6 stabilizes a magnetic structure that brings on spontaneous polarization.

Mn_2FeMoO_6, prepared at 1623 K under 8 GPa, crystallizes in the non-centrosymmetric Ni_3TeO_6-type ($R3$) structure as determined from combined refinements of powder synchrotron X-ray (PSXD) and neutron diffraction (PND) data (Section 2 of SI). There are two crystallographically independent Mn ions (Mn1 and Mn2) at the A-sites; Fe and Mo are ordered over the B-sites. No oxygen deficiency was observed on the two oxygen positions (O1 and O2). The presence of cationic antisite disorder was also examined, with the best refinement indicating about 7% B-site Fe/Mo disorder, yielding the nominal composition: $Mn_2(Fe_{0.93(1)}Mo_{0.07(1)})(Mo_{0.93(1)}Fe_{0.07(1)})O_6$ (Table S1). No Mn/Fe disordering was observed during the refinements. The crystal structure along the c-axis is displayed in Figure 1a. The $Mn1O_6/MoO_6$ and $Mn2O_6/FeO_6$ face-sharing octahedral pairs along the c-axis form zigzag chains through edge-sharing with edge-shared $Mn1O_6/FeO_6$ and $Mn2O_6/MoO_6$ octahedral pairs in the ab-plane. The cations near the centers of the face-shared octahedral pairs are displaced by electrostatic repulsions (see the very large displacements in $Mn1O_6/MoO_6$ and $Mn2O_6/FeO_6$ octahedral pairs in Figure 1b and c) and cause large octahedral distortions comparable to those in $LiNbO_3$ (Table S2), in which the extended structure displays a polar moment along the c-axis. The ordering of Fe and Mo over the B-sites renders different atomic displacements (d_{Mn2} and d_{Mn1} in Figure 1b and c) of their face-shared pairs and conclusively accounts for the spontaneous polarization (P_S). The polar
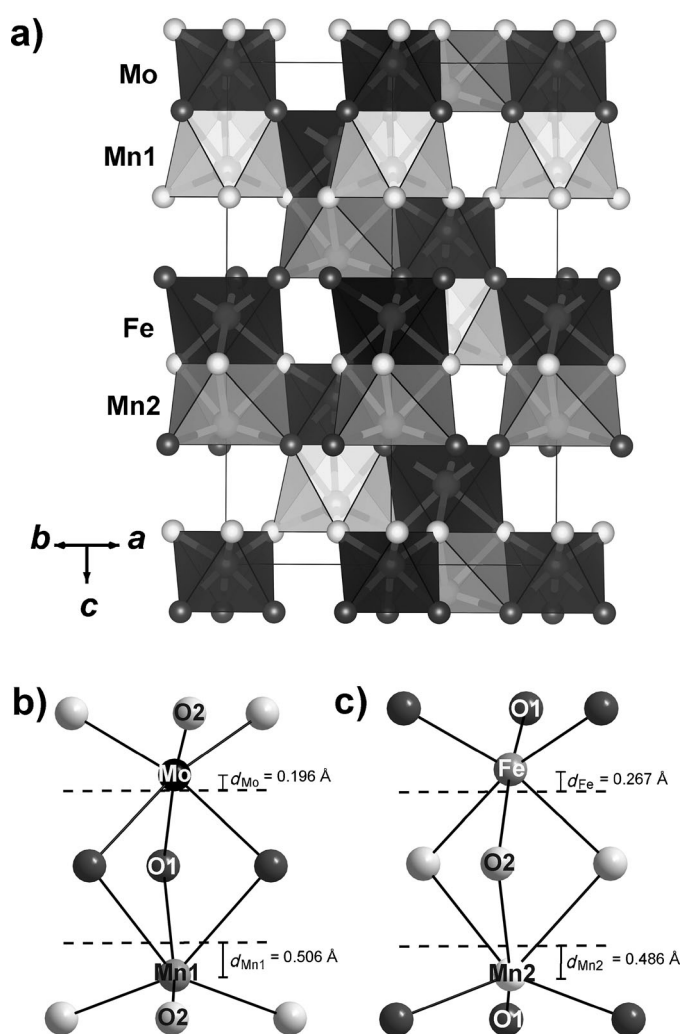

Figure 1. a) Crystal structure of Mn_2FeMoO_6 viewed along the [110] direction. b) and c) Enlarged views of the face-sharing $Mn1O_6/MoO_6$ and $Mn2O_6/FeO_6$ octahedral pairs along the c-axis to show the distortions and atomic displacements from half-way between the c-axis oxygen planes marked by dashed lines. $d_{Mn1} = 0.506$ Å, $d_{Mo} = 0.196$ Å, $d_{Mn2} = 0.486$ Å, $d_{Fe} = 0.267$ Å.

structure of Mn_2FeMoO_6 is directly confirmed by the active SHG response as shown in Figure S5. The crystal structure analysis together with the bond valence sums (BVS) calculations (Table S2) indicate that the formal oxidation states are Mn^{2+} (d^5), Fe^{3+} (d^5), and Mo^{5+} (d^1), as further confirmed by the X-ray absorption near-edge spectroscopic (XANES) studies (Section 4 of SI).

Figure 2a shows the evolution of magnetic susceptibility χ_{dc} versus T for Mn_2FeMoO_6. When the temperature is lowered from 400 K, the sample undergoes a paramagnetic to ferromagnetic transition with a sharp rise of the magnetization below a magnetic transition temperature (T_C) of ca. 350 K. A more precise $T_C = 337$ K can be estimated from the inflection point in the $d\chi_{dc}/dT$ versus T curve (top inset of Figure 2a). The high-temperature $1/\chi_{dc}$ versus T plot (bottom inset of Figure 2a) shows a deviation from the Curie–Weiss law but can be nicely fitted by the Néel model
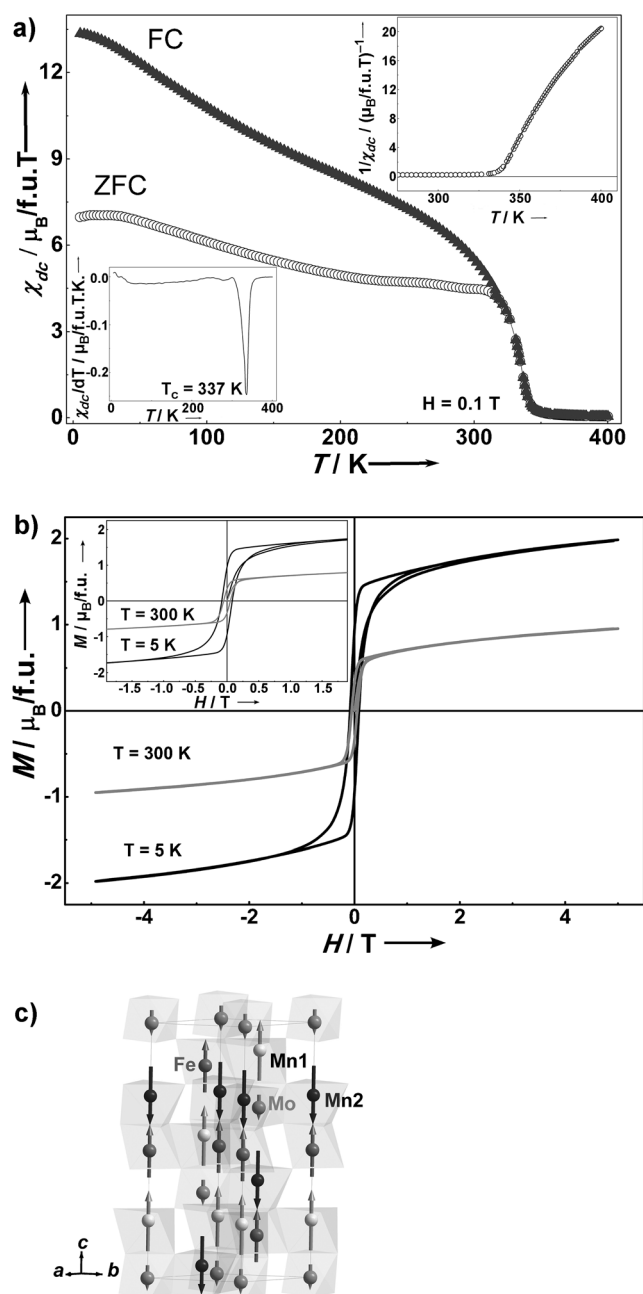
Figure 2. a) χ_{dc} versus T in the zero-field cooled as well as field cooled modes from 5 to 400 K with H = 0.1 T; the bottom (left) inset shows the $d\chi_{dc}/dT$ versus T curve; the top (right) inset shows the $1/\chi_{dc}$ versus T curve, which could be fitted to the Néel model for a two-sublattice ferrimagnet at higher temperature. b) M versus H curves at $T = 5$ and 300 K; the inset shows the expanded region between −1.5 and 1.5 T, showing clear hysteresis loops at both temperatures. c) Magnetic structure at 10 K refined from PND data demonstrating the spin polarization, the net magnetic moment $M = m(Mn1) + m(Fe) - m(Mn2) - m(Mo)$.

$\left(\frac{1}{\chi} = \frac{1}{\chi_0} + \frac{T}{C} - \frac{\sigma}{T - \theta}\right)$ for a two-sublattice ferrimagnet (black line in top inset of Figure 2a),[14] giving $\chi_0 = 0.016(1)$ emu mol^{-1} Oe, $C = 14.4(2)$ emu K mol^{-1} Oe, $\sigma = 8329(4)$ mol Oe emu^{-1} K, and $\theta = 239.9(1)$ K. From the value of C, we could estimate an effective magnetic moment $\mu_{eff} = 10.7\,\mu_B$, which is

close to the calculated spin-only moment per formula unit ($\mu_{calc.} = 10.4\,\mu_B$). The ferrimagnetism is also confirmed by the isothermal magnetization curves recorded at 5 and 300 K (Figure 2b). The PND data show magnetic contributions in some low-angle reflections at both 10 and 300 K. The magnetic intensities at 10 K have been refined in a model that considered the following ferrimagnetic arrangement (see Table S1): in the face-sharing $Mn1O_6/MoO_6$ pairs the spins of Mn1 ($4.0(3)\,\mu_B$) are along the c direction and antiparallel to the Mo moments ($-1.1(1)\,\mu_B$). Similarly, in the face-sharing $Mn2O_6/FeO_6$ pairs, the spins of Mn2 ($-3.8(2)\,\mu_B$) and Fe ($3.4(5)\,\mu_B$) are also antiparallel along the c axis. In the ab planes, Mn1 and Fe spins order ferromagnetically in one layer, whereas those of Mn2 and Mo in the next layer also order ferromagnetically, but antiparallel to those of Mn1 and Fe. The magnetic structure is shown in Figure 2c. The net magnetic moment from PND refinements ($2.5(3)$ and $0.81(8)\,\mu_B$ for 10 and 300 K, respectively) is comparable to the saturation magnetization in Figure 2b (≈ 1.98 and $0.95\,\mu_B$ mol^{-1} at 5 and 300 K, respectively).

The plot of resistivity ρ versus T for Mn_2FeMoO_6 at H = 0 T (Figure 3) is characteristic of semiconducting behavior with a resistivity value of around 20 Ω cm at 300 K. The resistivity becomes too high to measure below 80 K. In the entire temperature range between 80 and 300 K, the resistivity follows a Mott's variable range hopping (VRH)[15] conduction mechanism:

$$\rho = \rho_0 \exp\left[\left(\frac{T_0}{T}\right)^{1/4}\right]$$

as seen in the linear fit in the plot of $\ln\rho$ versus $1/T^{1/4}$ (black line in inset of Figure 3). The fitting allowed us to extract the parameters T_0 and ρ_0, 1.15×10^8 K and $2.6 \times 10^{-10}\,\Omega$ cm, respectively, which are similar to the observed values in other transition metal oxides.[16] Thus, Mn_2FeMoO_6 is a ferrimagnetic VRH semiconductor.

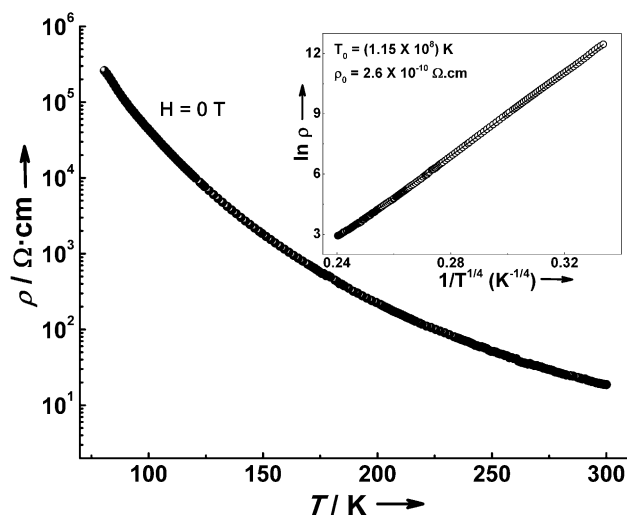**Figure 3.** ρ versus T plot at zero-field showing semiconductor behavior. The inset shows the linear fit to the plot of $\ln\rho$ versus $1/T^{1/4}$, indicating Mott's VRH conduction mechanism.

DFT calculations (Section 6 of SI) confirmed the high-spin nominal d^5 state of both Fe^{3+} and Mn^{2+}, and that of Mo^{5+} to be nominally d^1. A somewhat large value of magnetic moment (≈ 0.10–$0.12\ \mu_B$) is found to reside at the O site, suggesting strong d–p hybridization between the transition metals and O. The ferrimagnetic spin structure (cited as up-up-down-down along the zigzag chain) in Figure 2c is confirmed to be lower in energy than the ferromagnetic (spins of Mn, Fe, and Mo all aligned parallel) and ferrimagnetic (antiparallel alignment of Mn1 and Mn2, but parallel alignment of Fe and Mo, cited as up-up-down-up) solutions by a large energy difference of about 300 and 80 meV, respectively, which is consistent with PND data analysis. This suggests a very strong antiferromagnetic exchange between Mn1 and Mn2 and a moderately strong antiferromagnetic exchange between Fe and Mo. In Figure 4 the density of states (DOS) in the ground state (up-up-down-down magnetic configuration) supports the above conclusions. The magnetic as well as the conducting properties (the presence or absence of band gap) seem to be highly influenced by the assumed configuration of the Fe–Mo arrangement whereas the nominal valences remain unaffected, a fact well established for double perovskites.[17] This presumably explains the VRH semiconducting behavior dominated by disorder ($\approx 7\%$) as well as the experimental observation of a net moment of ca.
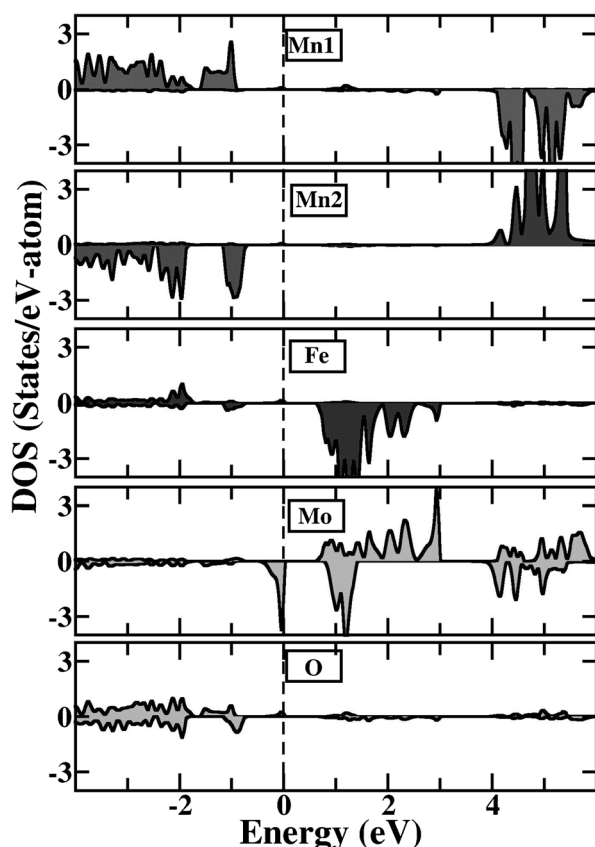
2.5 μ_B, which is highly suppressed compared to the theoretical estimate of 4.0 μ_B based on a perfectly ordered state, and also suggests possible resistivity tuning by controlling the Fe/Mo disordering degree.

The crystal structure of Mn$_2$FeMoO$_6$ breaks the polarization rule, because known polar perovskite-related and corundum-based compounds contain ions with either $(n-1)$d^{10}ns^0, or d^0 electronic configuration,[11a] or at least one stereoactive lone pair.[3] To the best of our knowledge, polar ε-Fe$_2$O$_3$ is the only exception with only d^n ($0 < n < 10$) ions, but its crystal structure is very different. Moreover, it still remains a challenge to prepare large amounts of pure, thermally stable ε-Fe$_2$O$_3$.[12c] First principles total energy calculations of Mn$_2$FeMoO$_6$ based on the Fe/Mo arrangements suggest that the Fe/Mo ordered configuration is energetically preferred over the segregated and mixed configuration (Section 6 of SI), by the energy difference of 600 and 150 meV, respectively, when the magnetism is turned on. The ordered ilmenite structure (Figure S1d) also has ordered Fe–Mo, but is about 30 meV/f.u. higher in energy than the Ni$_3$TeO$_6$ structure, due to the large size mismatch between Mn^{2+} and Fe^{3+}.[18] Thus, it is clear that the magnetic structure stabilizes the polarization in Ni$_3$TeO$_6$-type Mn$_2$FeMoO$_6$. The P_S was calculated to be ca. 68 μC cm^{-2}, suggesting a ferroelectric T_C around 1400 K according to the empirical relation between T_C and P_S.[19] Dielectric and polarization measurements also confirmed the ferrimagnetic semiconductor behavior (Figure S8), but do not evidence any ferroelectric transition-related anomaly/component (Figure S9). However, this finding does not exclude the possibility of ferroelectricity in thin-film or single-crystal samples of this material as reported in a related sample of LN-type ferroelectric ZnSnO$_3$ thin film,[20a] which also shows no dielectric anomaly in the bulk polycrystalline sample.[20b]

In conclusion, we showed for the first time that a non-centrosymmetric structure and spontaneous polarization can be stabilized in a corundum-based compound that orders ferrimagnetically above RT. Mn$_2$FeMoO$_6$ is truly unique in that the B-site cations order at the very high pressure and temperature of synthesis, so that the very strong magnetic interactions (d^5/d^1) in the Fe–Mo-ordered phase stabilize the magnetic structure of lowest energy that brings on the polarization. Thus, this system is different from the LnMnO$_3$ perovskites,[5] since the Mn$_2$FeMoO$_6$ is magnetically ordered, non-centrosymmetric, and polar already at RT. Also according to first-principle calculations, the magnetic structure is lower in energy than related centrosymmetric and disordered phases, and the polarization, induced by this magnetic structure, is high. This finding is significant in the search for new multiferroics and for the development of the field of spintronics, because there are very limited known single-phase RT magnetoelectric materials to date,[3] and some still with controversy.[21] This discovery provides intriguing strategies to discover new practical magnetoelectric materials by incorporating strong magnetic ions at all cationic sites of A$_2$BB'O$_6$.

Figure 4. DFT calculations of DOS in the ground-state (up-up-down-down) magnetic configuration projected to Mn1, Mn2, Fe, Mo, and O sites. This magnetic configuration is found to be energetically favorable over the ferrimagnetic (up-up-down-up) and ferromagnetic configurations.

[1] N. A. Spaldin, M. Fiebig, *Science* **2005**, *309*, 391–392.

[2] W. Eerenstein, M. D. Mathur, J. F. Scott, *Nature* **2006**, *442*, 759–765.

[3] J. Wang, et al., *Science* **2003**, *299*, 1719–1722 (see the Supporting Information).

[4] N. Ikeda, et al., *Nature* **2005**, *436*, 1136–1138 (see the Supporting Information).

[5] T. Kimura, T. Goto, H. Shintani, K. Ishizaka, T. Arima, Y. Tokura, *Nature* **2003**, *426*, 55–58.

[6] a) R. Ramesh, N. A. Spaldin, *Nat. Mater.* **2007**, *6*, 21–29; b) J. H. Lee, et al. *Nature* **2010**, *466*, 954–958 (see the Supporting Information).

[7] T. Varga et al., *Phys. Rev. Lett.* **2009**, *103*, 047601 (see the Supporting Information).

[8] P. S. Halasyamani, K. R. Poeppelmeier, *Chem. Mater.* **1998**, *10*, 2753–2769.

[9] a) J. M. Rondinelli, C. J. Fennie, *Adv. Mater.* **2012**, *24*, 1961–1968; b) A. T. Mulder, N. A. Benedek, J. M. Rondinelli, C. J. Rennie, *Adv. Funct. Mater.* **2013**, *23*, 4810–4820; c) N. A. Benedek, C. J. Fennie, *Phys. Rev. Lett.* **2011**, *106*, 107204; d) N. A. Benedek, *Inorg. Chem.* **2014**, *53*, 3769–3777.

[10] A. A. Belik, T. Furubayashi, H. Yusa, E. Takayama-Muromachi, *J. Am. Chem. Soc.* **2011**, *133*, 9405–9412.

[11] a) R. E. Cohen, *Nature* **1992**, *358*, 136–138; b) N. A. Hill, *J. Phys. Chem. B* **2000**, *104*, 6694–6709.

[12] a) Y. Kitagawa, Y. Hiraoka, T. Honda, T. Ishikura, H. Nakamura, T. Kimura, *Nat. Mater.* **2010**, *9*, 797–802; b) G. T. Rado, V. J. Folen, *Phys. Rev. Lett.* **1961**, *7*, 310–311; c) J. Tuček, R. Zbořil, A. Namai, S. i. Ohkoshi, *Chem. Mater.* **2010**, *22*, 6483–6505.

[13] a) M. R. Li, et al. *Angew. Chem.* **2013**, *125*, 8564–8568; *Angew. Chem. Int. Ed.* **2013**, *52*, 8406–8410 (see the Supporting Informatioin); b) Y. S. Oh, S. Artyukhin, J. J. Yang, V. Zapf, J. W. Kim, D. Vanderblt, S. W. Cheong, *Nat. Commun.* **2014**, *5*, 3201.

[14] L. Néel, *Ann. Phys.* **1948**, *3*, 62.

[15] N. F. Mott, *Conduction in non-crystalline materials*, 2nd ed., Clarendon, Oxford, **1993**.

[16] J. Fontcuberta, B. Martínez, A. Seffar, S. Piñol, J. L. García-Muñoz, X. Obradors, *Phys. Rev. Lett.* **1996**, *76*, 1122–1125.

[17] T. Saha-Dasgupta, D. D. Sarma, *Phys. Rev. B* **2001**, *64*, 064408.

[18] R. Shannon, *Acta Crystallogr. Sect. A* **1976**, *32*, 751–767.

[19] S. C. Abrahams, S. K. Kurtz, P. B. Jamieson, *Phys. Rev.* **1968**, *172*, 551–553.

[20] a) J. Y. Son, G. Lee, M. H. Jo, H. Kim, H. M. Jang, Y. H. Shin, *J. Am. Chem. Soc.* **2009**, *131*, 8386–8387; b) Y. Inaguma, D. Sakurai, A. Aimi, M. Yoshida, T. Katsumata, D. Mori, J. Yeon, P. S. Halasyamani, *J. Solid State Chem.* **2012**, *195*, 115–119.

[21] W. Eerenstein, F. D. Morrison, J. Dho, M. G. Blamire, J. F. Scott, N. D. Mathur, *Science* **2005**, *307*, 1203–1203.